平成１１年度　修士論文

A Study on the Fluctuation of the Terrestrial Ionosphere for the Radio Occultation Measurements of Planetary Ionospheres

(惑星電離圏電波掩蔽観測のための地球電離圏擾乱に関する研究)

指導教官　小山 孝一郎 教授

東京大学大学院

理学系研究科地球惑星物理学専攻

野口 克行

Abstract

The fluctuation of the terrestrial ionosphere, which is a serious error source when we try to obtain the information on planetary ionospheres by the radio occultation measurement, is focused on in this study. We are preparing for the radio occultation measurements of the Martian atmosphere and the lunar ionosphere by using the spacecrafts Nozomi and Selene, respectively. By using the radio occultation method, we can measure the electron densities in planetary ionospheres. The phase of the radio wave transmitted from the spacecraft to the Earth is perturbed when the radio wave passes through the planetary ionosphere. The electron density profile can be derived from the phase perturbation.

The information on the nightside ionosphere of Mars is based on the observations by the Mars 4 and 5 and the Viking orbiter. The detection of the lunar ionosphere by radio occultation technique was reported in the Luna 22 mission. Since the phase shift caused by the fluctuation of the terrestrial ionosphere is comparable to those by the Martian nightside ionosphere and the lunar ionosphere, the detection of these ionospheres is difficult in general. The fluctuation of the terrestrial Total Electron Content (TEC) along the ray path between the spacecraft and the receiving station is estimated from two coherent signals transmitted from several Global Positioning System (GPS) satellites. We can obtain the TEC information over Japan from the GPS network of the Geographical Survey Institute (GSI) in Japan, GPS Earth Observation Network (GEONET).

The possibility of the detection of the Martian nightside ionosphere and the lunar ionosphere at each local time is investigated for the summer and winter cases by using the TEC data obtained by the GPS network. The result indicates that the Martian nightside ionosphere and the lunar ionosphere can be measured if we choose suitable conditions of the terrestrial ionosphere for the measurement and monitor the fluctuation of the terrestrial ionosphere along the ray path of the radio occultation by using the GPS network.

There are several ways to estimate the TEC fluctuation of the terrestrial ionosphere by using the GPS network. In general, it is difficult to find a GPS satellite-ground receiver pair whose ray path is close to the ray path of the radio occultation measurement of the planetary atmosphere. Therefore, we develop a method to estimate the TEC fluctuation of the terrestrial ionosphere along the ray path of the radio occultation by many GPS satellite-ground receiver pairs. The feasibility of this method is tested by regarding one GPS satellite as the Nozomi or Selene spacecraft. A qualitatively good agreement between the true TEC and the estimated TEC was obtained by this method.

Contents

1 Introduction

1.1 Radio occultation measurements by Nozomi and Selene

The Japanese Mars spacecraft Nozomi was launched on July 4th, 1998, and will be put into the Mars orbit in 2004. Radio occultation measurement is one of the scientific objectives of the Nozomi mission. We have also a plan to carry out a radio occultation measurement using the lunar spacecraft SELenological and ENgineering Explorer (Selene), which will be launched in 2003.

Radio occultation measurements give us the information on the aeronomy of the planets. The measurement is carried out by using a spacecraft which emits unmodulated radio waves to the Earth [*Fjeldbo et al.,* 1965]. The phases of radio waves are perturbed when the rays pass through the planetary atmosphere. The antenna on the earth receives the radio wave. The density profiles of the neutral atmosphere and electrons will be derived from the phase perturbation assuming the spherical symmetry of the atmosphere [*Phinney et al.,* 1968; *Fjeldbo et al.,* 1971].

Radio occultation measurements can be carried out in both "1-way mode" and "2-way mode". In 1-way mode, the spacecraft emits unmodulated radio waves which are generated by an on-board oscillator. The onboard oscillator must be very stable in this case. In 2-way mode, on the other hand, the receiver on the spacecraft is phase-locked to the uplink signal which is generated by the stable oscillator on the earth. The spacecraft transponder generates the downlink signal from the uplink signal coherently.

We often use more than one frequency. The effect of the neutral atmosphere on the frequency is proportional to the nominal frequency. The errors due to the fluctuation of the onboard oscillator and the incorrect orbital information are also proportional to the nominal frequency. The effect of plasma is, on the other hand, inversely proportional to the nominal frequency. By using two frequencies, we can distinguish the effect of plasma from other effects.

In the Nozomi mission, we were to carry out measurements with S-band (2.3 GHz) and X-band (8.4 GHz) signals in 1-way mode using a stable onboard oscillator, so-called Ultra Stable Oscillator (USO). Unfortunately, however, the onboard S-band transmitter and the USO were turned off due to a trouble of power supply, thus we can not use the S-band signal and the USO. We are forced to carry out measurements in 2-way mode using S-band signal for the uplink and X-band for the downlink.

In the Selene mission, we will carry out measurements using an ordinary oscillator, whose frequency stability is 1.0×10^{-9} rms s^{-1} in the short term, since the spacecraft dose not have USO. It will be carried out in 1-way mode using S-band

(2.3 GHz) and X-band (8.4 GHz) for the downlink.

The data recording system at Usuda Deep Space Center (UDSC) is illustrated in Figure 1. The radio waves from the spacecraft are mixed with a local signal to cancel out the predicted Doppler shift due to the relative motion between the spacecraft and the receiver on the earth. By this mixing operation, the frequency of the signal from the spacecraft is converted down to the vicinity of 20 kHz. This analog signal is digitally recorded to CD-ROM media with 16 bit quantization and a sampling rate of 80 kHz. The data processing procedure is described in Appendix A.

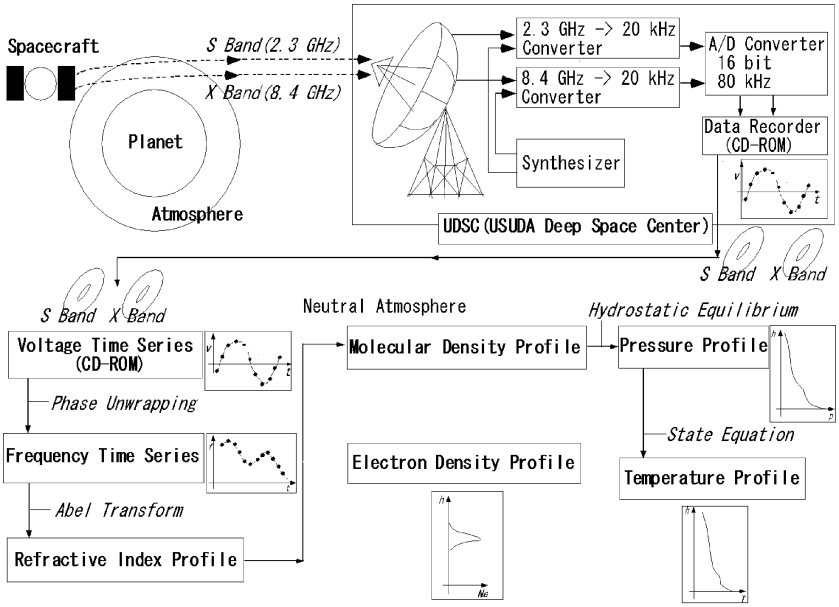

Figure 1: Data recording system at Usuda Station and the data processing procedure.

1.2 Previous radio occultation measurements of the Martian ionosphere and the lunar ionosphere

The previous radio occultation measurements at Mars are listed in Table 1. In the missions using one frequency, successful observations of the ionosphere are limited to entry occultations in 2-way mode (Mariner 4, 6, 7, 9). The Viking mission, which used two frequencies in 1-way mode, successfully observed the ionosphere in both entry and exit occultations.

The observations of the nightside ionosphere of Mars are quite few, because its electron density is too low to be detected [*Zhang et al.*, 1990]. The information on

Table 1: Radio occultation measurements at Mars

Spacecraft	Year	Method	Uplink	Downlink	Orbit	Note
Mariner 4 [*Fjeldbo et al.,* 1968]	1965	2-way (entry) 1-way (exit)	2.3 GHz	2.3 GHz	flyby	The first spacecraft to Mars. Only an entry session was successful for the ionosphere.
Mariner 6, 7 [*Hogan et al.,* 1972]	1969	2-way (entry) 1-way (exit)	2.3 GHz	2.3 GHz	flyby	
Mariner 9 [*Kliore et al.,* 1973]	1972	2-way (entry) 1-way (exit)	2.3 GHz	2.3 GHz	orbiter	The first orbiter to Mars.
Viking 1, 2 [*Lindal et al.,* 1979]	1976	2-way (entry) 1-way (exit)	2.3 GHz	2.3 GHz, 8.4 GHz	orbiter	
Mars 4, 5 [*Savich et al.,* 1976]	1974	1-way (exit)		0.9GHz 2.8GHz	flyby (Mars 4) orbiter (Mars 5)	
Mars Global Surveyor [*Hinson et al.,* 1999]	1997	1-way		8.4 GHz	orbiter	On observation. Neutral atmosphere is mainly observed.

the nightside ionosphere of Mars is based on the observations by the Mars 4 and 5 and the Viking orbiter. Two nightside profiles were obtained in the Mars 4 and 5 missions, and 19 nightside profiles were obtained in the Viking mission. *Savich et al.* [1976] showed the peak electron density of 5×10^3 cm^{-3} at altitudes of 110-130 km and the existence of an additional peak above the main one on the nightside from the measurements by Mars 4 and 5. Their evaluation of the time constant of recombination do not allow the persistence of the ionosphere produced by solar UV in daytime. This suggests that there must be other sources of nightside plasma. They also mention the possibility of the existence of plasma near the surface, but such a low-altitude plasma layer was not observed by the Viking mission.

The mechanism for maintaining the nightside ionosphere of Mars is thought to be similar to that of Venus. The main sources of the nightside ionosphere of Venus are thought to be the transport of atomic ions from the dayside [*Knudsen et al.,* 1980] and the electron precipitation to the nightside atmosphere [*Knudsen et al.,* 1985]. The transport from the dayside almost disappears at low solar activity while the electron precipitation exists also at low solar activity [*Knudsen,* 1992].

By analogy with Venus, we expect the existence of the transport from the dayside to the nightside and the electron precipitation to the nightside atmosphere also on Mars. In situ measurements of the nightward transport have not been done, but the electron precipitation in the vicinity of Mars was detected by HARP instrument onboard the Phobos 2 spacecraft [*Verigin et al.,* 1991; *Shutte et al.,*

1995]. The models of the nightside ionosphere of Mars were developed assuming the existences of the electron precipitation [*Verigin et al.,* 1991; *Haider et al.,* 1992] and the transport from the dayside [*Fox et al.,* 1993]. The measurement of the nightside ionosphere by the Nozomi radio occultation, together with other in situ plasma measurements, will reveal the source of the nightside plasma.

The detection of the lunar ionosphere by radio occultation technique was reported in the Luna 22 mission [*Vyshlov,* 1976]. They showed the peak electron concentrations of 500-1000 cm^{-3} at altitudes of 5-10 km above the sunlit lunar surfaces.

Photoionization theories cannot explain the thick ionosphere reported by the Luna 22 mission. Assuming that the ionosphere is composed of the photoelectrons from the material of the lunar sunlit surface, the electron layer would exist only within several tens of meters above the surface [*Reasoner et al.,* 1972]. Such a photoelectron layer was observed by the Apollo missions [*Stern,* 1999]. Assuming that the ionosphere is composed of the photoelectrons supplied by the ionization of neutral gases, the electron layer would be removed by solar wind because the time constant of ionization is much longer than that of the pick-up process [*Bauer,* 1996]. The measurement of the lunar ionosphere by the Selene radio occultation will improve our knowledge on the source of plasma near the moon.

1.3 The effect of the terrestrial ionosphere on the radio occultation measurement

Radio occultation measurements have several error sources:

1. Fluctuation of the plasma density in the terrestrial ionosphere.
2. Fluctuation of the plasma density in the interplanetary space.
3. Fluctuation of the frequency of oscillator.
4. Recording error at the ground station.
5. Deviation of the atmospheric structure from spherical symmetry.

The effect of the interplanetary plasma on the radio occultation measurements can be negligible if the ray path is far from the sun, because the power of the fluctuations in the time scale of the radio occultation measurement is small [*Woo et al.,* 1979]. Here we examine the first error source, the density fluctuation in the terrestrial ionosphere. The density fluctuation in the terrestrial ionosphere causes the fluctuation of the amplitude and the phase of the received signal. Since phase shift is the primary source of information in our experiment, we focus on

the phase fluctuation caused by the disturbances in the terrestrial ionosphere. It will be shown in Section 2 that the phase fluctuation caused by the terrestrial ionosphere is comparable with those by the Martian nightside ionosphere and the lunar ionosphere.

It should be noted that only short time scale fluctuations become serious error sources, since long time scale fluctuation can be removed by extrapolating the data before occultation. An example of the elimination of the long time scale variation in a previous work is shown in Figure 2 [*Mizuno,* 1991]. The extrapolation of the phase shift before the occultation was used to remove the long time scale variation. The time scale of the extrapolation was several minutes in this case.

The fluctuation of the terrestrial Total Electron Content (TEC) along the ray path between the spacecraft and the receiving station will be estimated from the signals transmitted from several Global Positioning System (GPS) satellites. Two coherent signals from a GPS satellite enables us to estimate the TEC along the ray path between the GPS satellite and the receiving station. The characteristics of the TEC fluctuation have been investigated from the data obtained by the International GPS Service for Geodynamics (IGS) in the equatorial [*Aarons et al.,* 1996], mid-latitude [*Doherty et al.,* 1994], and auroral-latitude [*Aarons,* 1997] regions. The revealed characteristics are as follows:

1. Maximum occurrence and magnitude of the phase scintillation are observed in the nighttime [*Aarons et al.,* 1996; *Doherty et al.,* 1994].

2. The phase scintillation takes place in high Kp index period rather than in low Kp index period [*Aarons et al.,* 1996; *Aarons,* 1997; *Doherty et al.,* 1994].

3. In the mid-latitude, the magnitude of the short term[1] (1 minute) phase scintillation is smaller than that of the long term (15 minutes) scintillation [*Doherty et al.,* 1994].

We can obtain the TEC information over Japan from the GPS network of the Geographical Survey Institute (GSI) in Japan, GPS Earth Observation Network (GEONET). The wave structure of the mid-latitude Traveling Ionospheric Disturbances (TID) in the nighttime was observed by GEONET [*Saito et al.,* 1998].

[1]The time scale of the radio occultation measurement is about several minutes. The "short term" means a short time scale compared with the time scale of the radio occultation measurement.

(a)

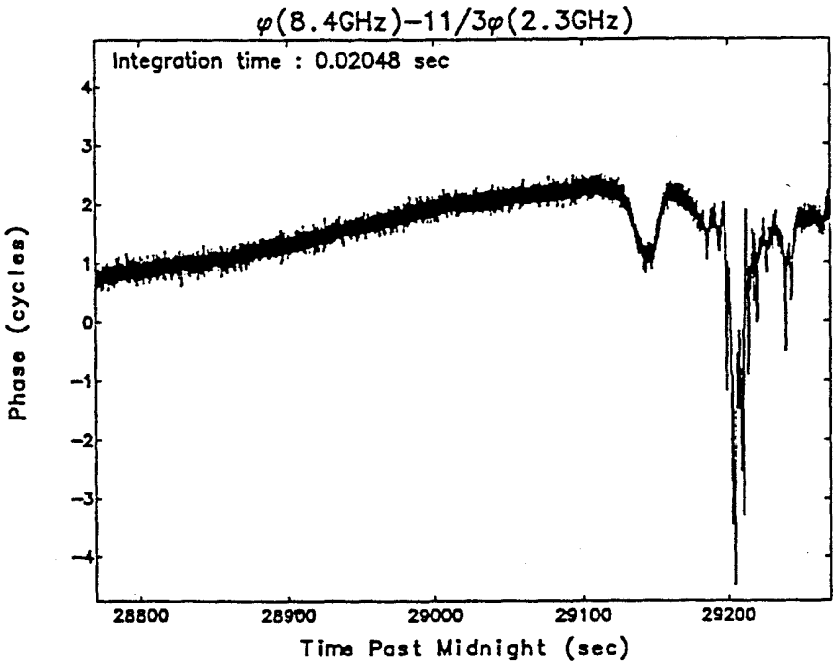

(b)

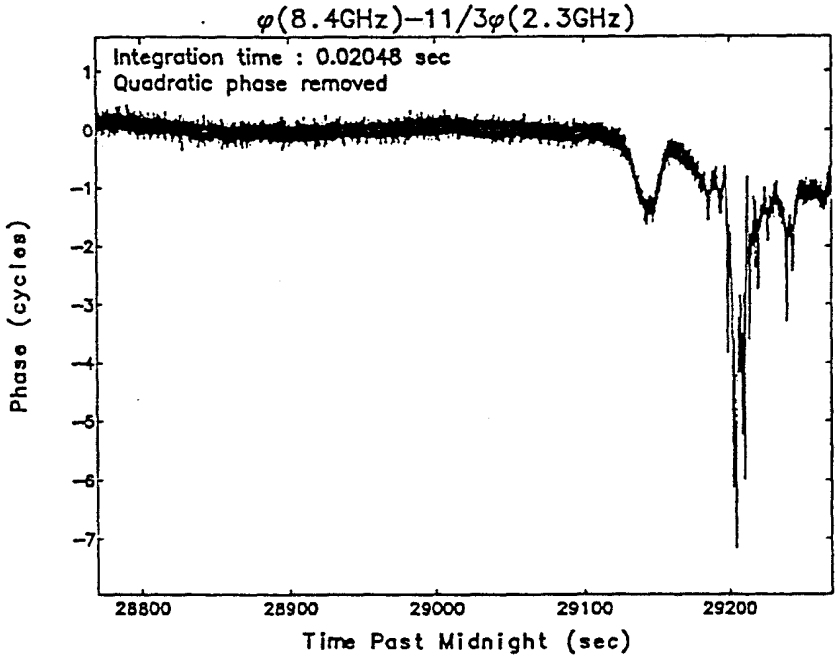

Figure 2: Phase shift by the Neptune ionosphere measured in the Voyager 2 mission. (a) Phase shift before the subtraction of a long time scale variation. (b) Phase shift after the subtraction. The figures are taken from *Mizuno* [1991].

The goals of this study are:

1. To compare the phase shifts by the Martian nightside ionosphere and the lunar ionosphere with the phase shift by the small-scale fluctuation of the terrestrial ionosphere.

2. To clarify the magnitude and the local-time dependence of the fluctuation of the terrestrial ionosphere over UDSC by analyzing the TEC data observed by the GPS network.

3. To develop a method to estimate the fluctuation of the terrestrial ionosphere along the ray path of the radio occultation by using the TEC data observed by the GPS network.

2 Phase shift due to planetary ionospheres

2.1 Principle of the phase shift due to plasma

The phase shift $\delta\phi$ due to plasma is

$$\delta\phi = \frac{1}{\lambda}\int(\mu - 1)dx, \tag{1}$$

where x is the distance along the ray path, λ is the wave length of the radio wave, and μ is the refractive index of plasma. Substituting (22) into (1), we get

$$\delta\phi = -40.3\frac{I}{cf_{USO}}, \tag{2}$$

where I is the total electron content along the ray path in units of m^{-2}, c is the light velocity in m s^{-1}, and f_{USO} represents the nominal frequency of the radio wave from the spacecraft in Hz. I is expressed as

$$I = \int N_e dx, \tag{3}$$

where N_e is the electron density of plasma. The frequency shift is the derivative of $\delta\phi$ with respect to time t, thus it is proportional to dI/dt. Since dI/dt is proportional to the spacecraft velocity, the frequency shift is proportional to the spacecraft velocity as well as the electron content.

We calculate the total electron content I along the ray path in the Martian ionosphere and the lunar ionosphere assuming that the spacecraft moves in a direction perpendicular to the ray path. By substituting the calculated I into (2), the phase and frequency shifts are obtained. We also calculate the phase shifts due to the fluctuation of the terrestrial ionosphere from GPS data in typical cases to compare them with the phase shifts by the Martian ionosphere and the lunar ionosphere.

2.2 Martian ionosphere

For the calculation of the phase shift by the Martian ionosphere, the dayside and nightside electron density profiles observed by the Viking mission are adopted (see Section 1.2). The adopted velocities of the spacecraft are the maximum and minimum velocities in the model orbit of Nozomi (Figure 3).

The phase shifts caused by the radio occultation of the Martian dayside and nightside ionospheres are shown in Figures 4 and 5, respectively. The phase shifts due to the fluctuation of the terrestrial ionosphere along the ray path are also shown for comparison. The density of the Martian dayside ionosphere is large

enough to be detected. On the other hand, the Martian nightside ionosphere is difficult to be detected when the spacecraft moves slowly, since the fluctuation of the terrestrial ionosphere is as large as the signature of the Martian nightside ionosphere.

2.3 Lunar ionosphere

For the calculation of the phase shift by the lunar ionosphere, the electron density profile observed by the Luna 22 mission is adopted (see Section 1.2). The adopted velocity is taken from the planned orbit of Selene (Figure 6).

The phase shifts caused by the radio occultation of the lunar ionosphere is shown in Figures 7. The phase shifts due to the fluctuation of the terrestrial ionosphere are also shown for comparison. When the terrestrial ionosphere is very calm, the phase shift due to the lunar ionosphere would be detected if the lunar ionosphere is as thick as the electron layer observed by Luna 22. Since we can carry out the measurement many times during the Selene mission, we will be able to show statistically whether the lunar ionosphere exists or not.

The maximum total electron content along the ray path, the maximum phase shift, and the time scale of the observations are summarized in Table 2. In order to discuss the feasibility of the measurements of the Martian nightside ionosphere and the lunar ionosphere in more detail, the properties of the fluctuation of the terrestrial ionosphere will be investigated in Section 3.

Table 2: Maximum total electron content along the ray path, maximum phase shift, and time scale of the observations.

Ionosphere	**I** $[\times 10^{16}$ **m**$^{-2}]$	**Phase shift [cycle]**	**Time scale**
Mars (nightside)	0.26	0.15	Several minutes
Moon*	0.05	0.03	Several tens seconds

*Very thick ionosphere reported by the Luna 22 mission is adopted.

(a)

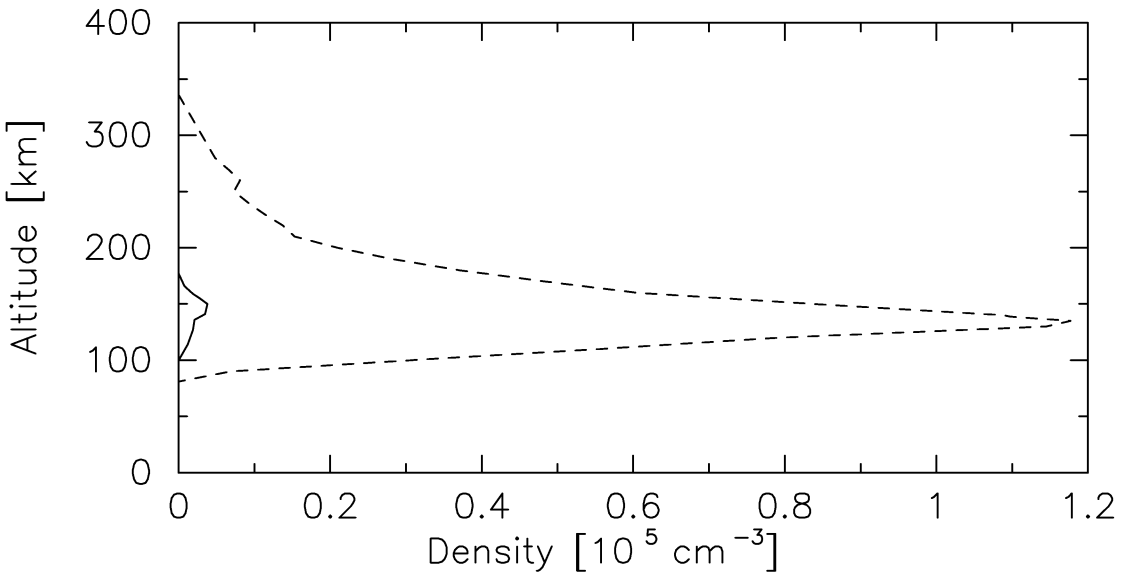

(b)

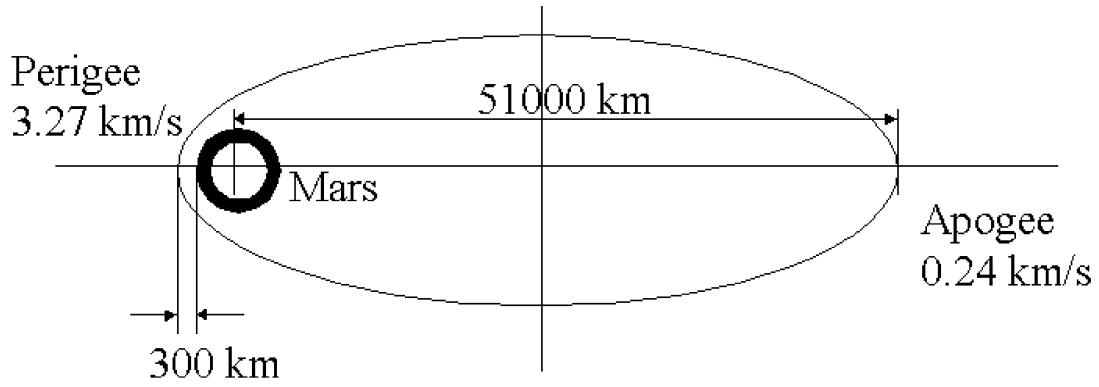

Figure 3: Calculation condition for the Martian ionosphere. (a) Electron density profiles measured by Viking. Dashed curve indicates the dayside profile and solid curve indicates the nightside profile [*Lindal et al.*, 1979]. (b) Planned orbit of Nozomi.

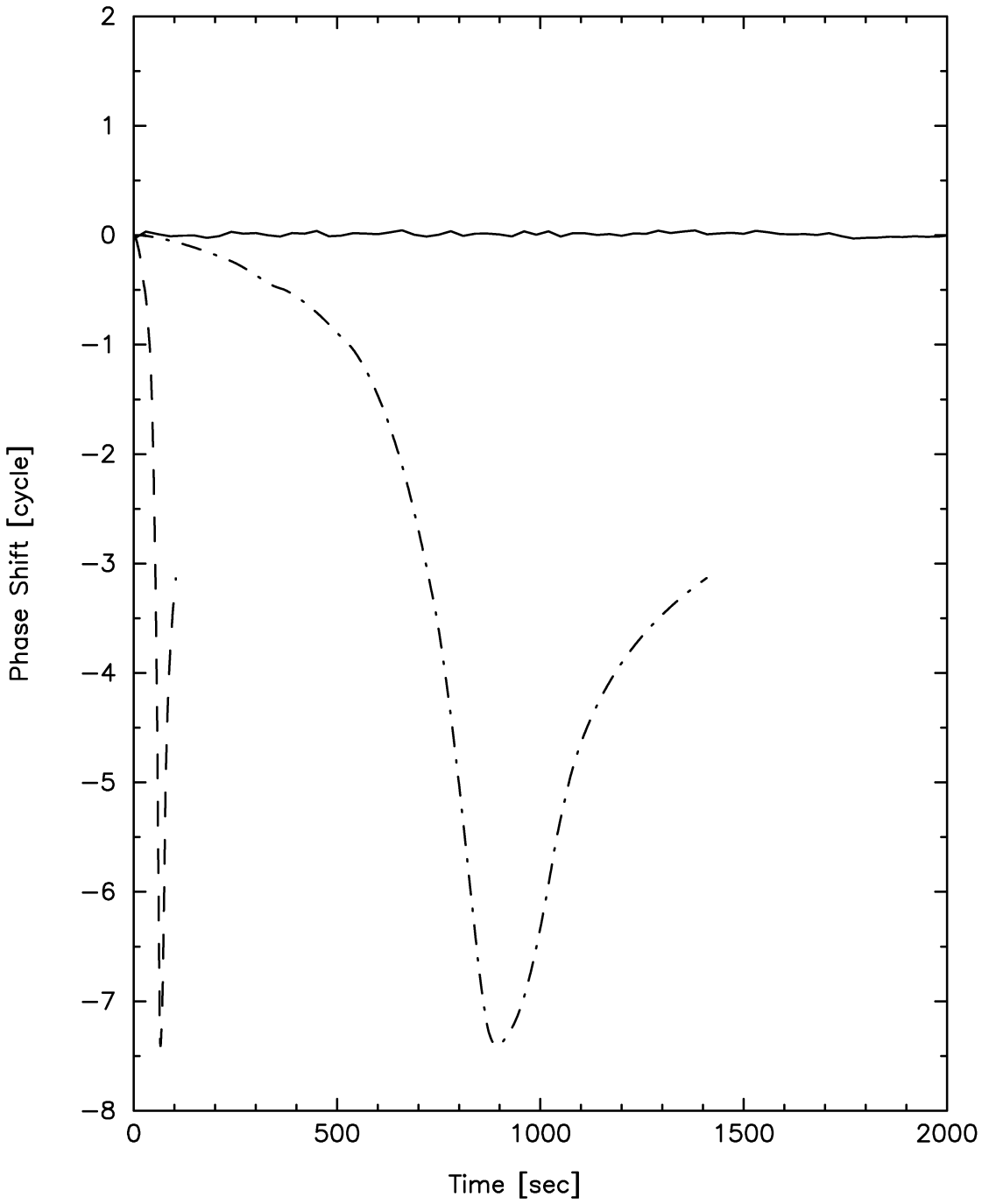

Figure 4: Phase shifts caused by the radio occultation of the Martian dayside ionosphere. Dashed curve and dot-dashed curve indicate the phase shifts when the velocity of the spacecraft is maximum (3.27 km s^{-1}) and minimum (0.24 km s^{-1}), respectively. Solid curve indicates the phase shift due to the fluctuation of the terrestrial ionosphere calculated from GPS data in a typical case (Section 3).

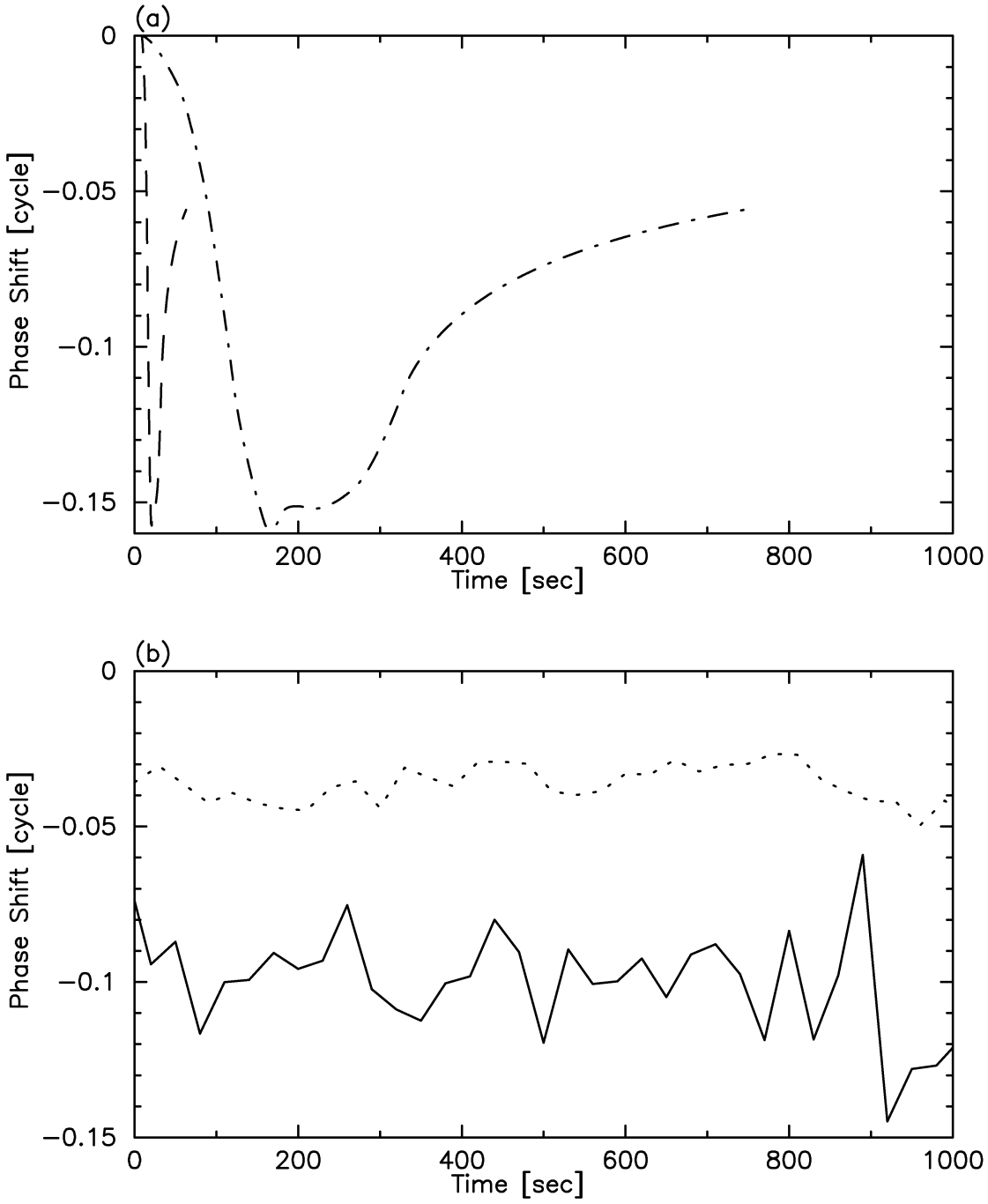

Figure 5: (a) Phase shifts caused by the radio occultation of the Martian nightside ionosphere. Dashed curve and dot-dashed curve indicate the phase shifts when the velocity of the spacecraft is maximum (3.27 km s^{-1}) and minimum (0.24 km s^{-1}), respectively. (b) Phase shifts due to the fluctuation of the terrestrial ionosphere calculated from GPS data. Solid and dotted lines indicate a larger and smaller fluctuations of the terrestrial ionosphere, respectively (Section 3).

(a)

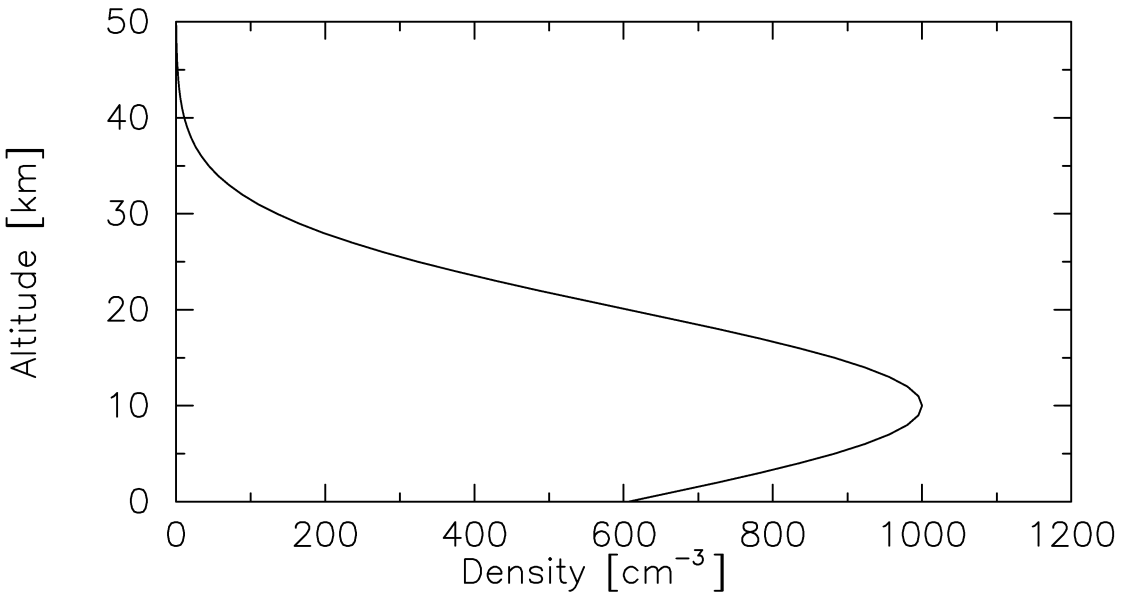

(b)

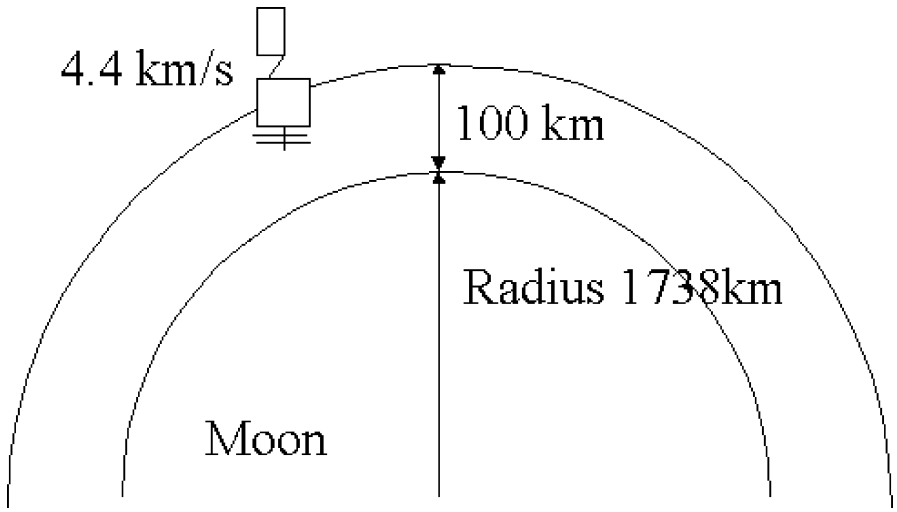

Figure 6: Calculation condition for the lunar ionosphere. (a) Electron density profile measured by Luna 22 [*Vyshlov et al.*, 1976]. (b) Planned orbit of Selene.

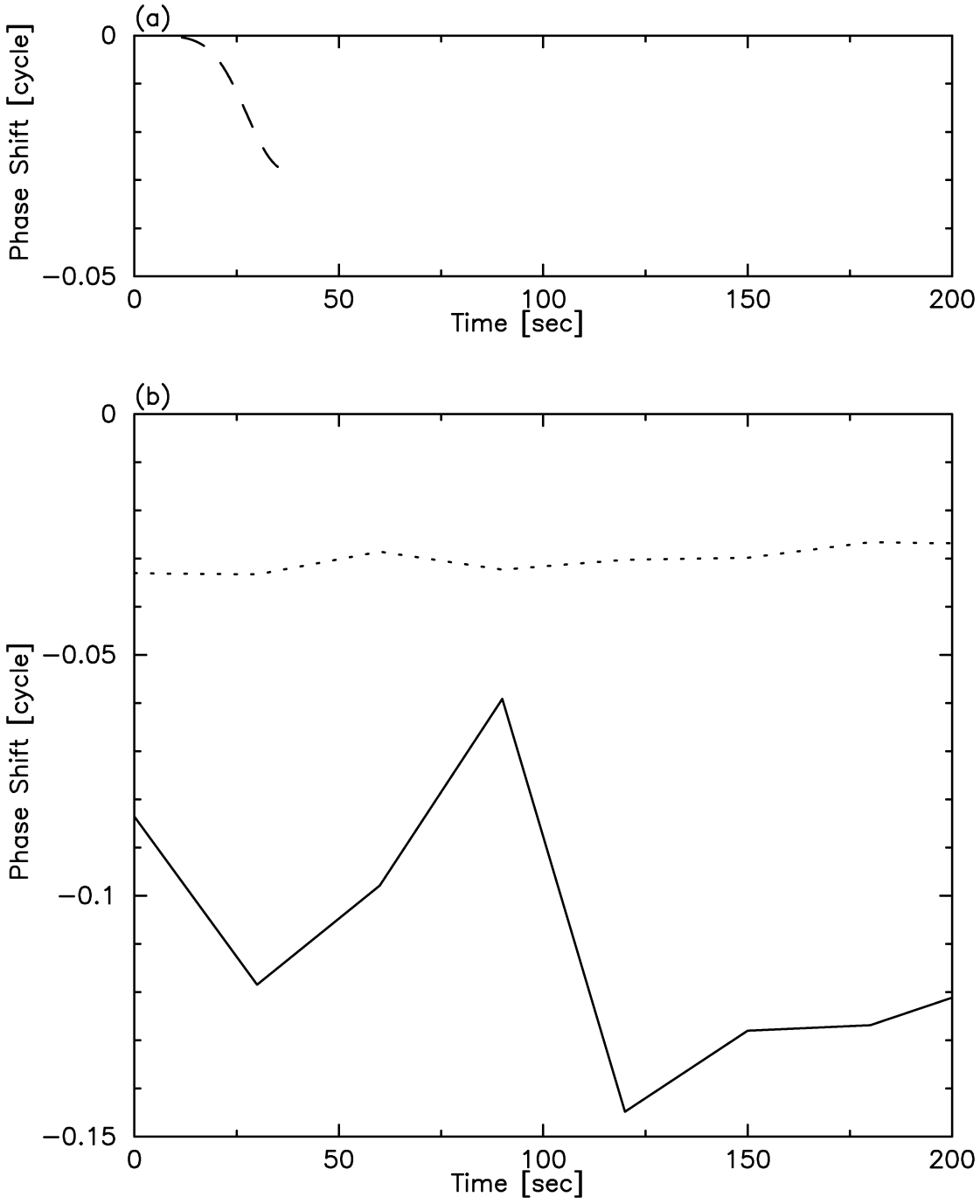

Figure 7: (a) Phase shift caused by the radio occultation of the lunar ionosphere. (b) Phase shifts due to the fluctuation of the terrestrial ionosphere calculated from GPS data. Solid and dotted lines indicate a larger and smaller fluctuations of the terrestrial ionosphere, respectively (Section 3).

3 Properties of the fluctuation of the terrestrial ionosphere

3.1 Method

The dependences of the fluctuation of the terrestrial ionosphere on local time and season are investigated by using the TEC data observed by the GPS network. We can obtain the terrestrial TEC along the ray path of GPS satellite-ground receiver pair as the raw data.

An offset peculiar to each GPS satellite-ground receiver pair is included in the raw TEC data. Since we are interested in the short time scale component of the fluctuation in the terrestrial ionosphere, the trend component due to the variation of the path length in the terrestrial ionosphere associated with the movement of the GPS satellite and long time scale variations is removed by subtracting the running average. By removing the trend component, the offset peculiar to the GPS satellite-ground receiver pair is also removed.

The typical amplitude of the short time scale fluctuation is evaluated by two methods. One method is to calculate the standard deviation of the fluctuation of the TEC every one hour after removing a long time scale variation which is obtained by 10 minutes running average. The other method is to calculate the power spectrum $P(f)$ of the fluctuation of the TEC and obtain the typical amplitude A as the root of the power:

$$A = \sqrt{\int_{f_1}^{f_2} P(f) df}, \tag{4}$$

where f_1 and f_2 are the maximum and minimum frequencies, respectively, to be considered.

The sampling interval of the TEC data is 30 seconds. The measurement error of the raw TEC value is less than 10^{14} m^{-2} [*Hernandez-Pajares et al.*, 1998]. The property of the observations used in the analysis is listed in Table 3.

Table 3: The property of the observations.

Receiver ID	0272 (near UDSC)
Date	Apr. 24, 1999 - Dec. 31, 1999 (249 days, there is a loss of a few days.)

3.2 Results

As we obtained similar results from above two methods, we show only the results which are obtained by the standard deviation method.

Before the analysis, we check whether there is any non-uniformity of the distribution of measurements in the field of view from the receiver. Figure 8 shows the distribution of the measurements every 6 hours. The measurements at low elevations are removed to avoid the effect of the fluctuation far from UDSC. It is concluded that the distribution of the observations above the elevation of 30° is nearly uniform.

The dependence of the activity of the fluctuation on Kp index is shown in Figure 9. The relation between the activity of the fluctuation and Kp index is not clear. However, we can not exclude the possibility of the dependence of the fluctuation activity on Kp index because the number of samples in high Kp period is not enough. In the present study, we use the data obtained under the condition that Kp index is in the range between 0 and 2−.

Figure 10 shows the dependence of the fluctuation amplitude of the terrestrial ionosphere on local time. The samplings are nearly uniformly distributed over local time. From June to August, the peak amplitude occurs between 2200 and 2300 LT. From September to October, any clear peak can not be seen. From November to December, there is a peak between 1200 and 1300 LT. The local time of the peak activity of the fluctuation changes with season.

The possibility of the detection of the Martian nightside ionosphere and the lunar ionosphere is investigated for the summer and winter cases using the above results. We regard the fluctuation of the terrestrial ionosphere as a noise. Then, the signal-to-noise ratio R is defined as

$$R = \frac{I_{planet}}{I_{earth}}, \tag{5}$$

where I_{planet} is the maximum total electron content along the ray path in the planetary ionosphere (see Section 2) and I_{earth} is the fluctuation of the total electron content of the terrestrial ionosphere. The detection possibility P at each local time is defined as

$$P = \frac{N_{SN}}{N_{all}} \times 100, \tag{6}$$

where N_{SN} is the number of samples whose R value is more than 2, 5, and 10, and N_{all} is the total number of samples at each local time.

Figures 11 and 12 are the results for the Martian nightside ionosphere and the lunar ionosphere, respectively. In both cases, December is more suitable for the measurement than July because of the smaller fluctuation of the terrestrial ionosphere in December. Daytime is suitable for the measurement in July, while nighttime is suitable for the measurement in December.

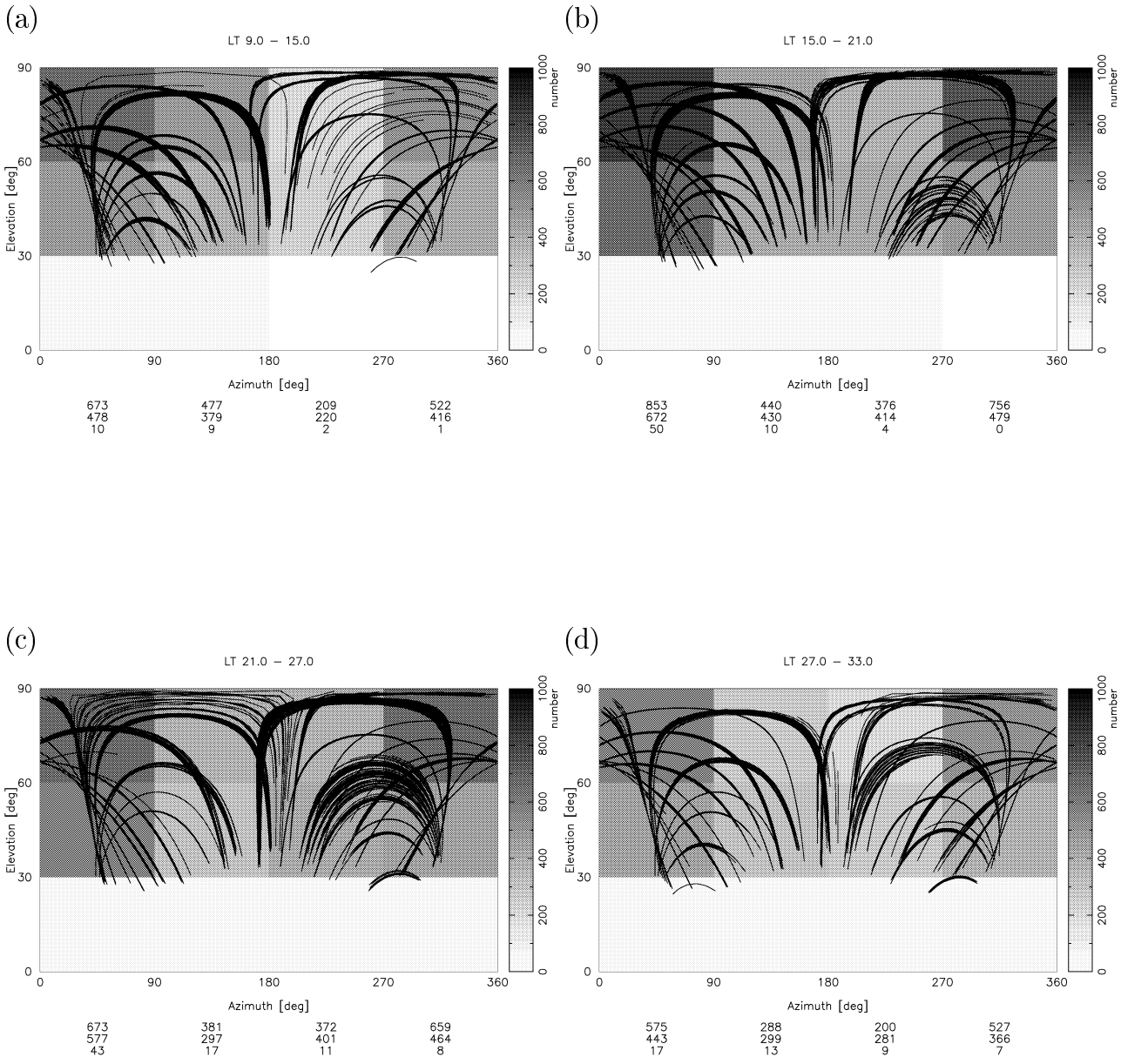

Figure 8: Distribution of the observations by GPS satellites in the field of view from the receiver between (a) 0900 and 1500 LT, (b) 1500 and 2100 LT, (c) 2100 and 0300 LT, and (d) 0300 and 0900 LT. The brightness indicates the number of samplings in each area. Solid curves represent the orbits of the GPS satellites.

(a)

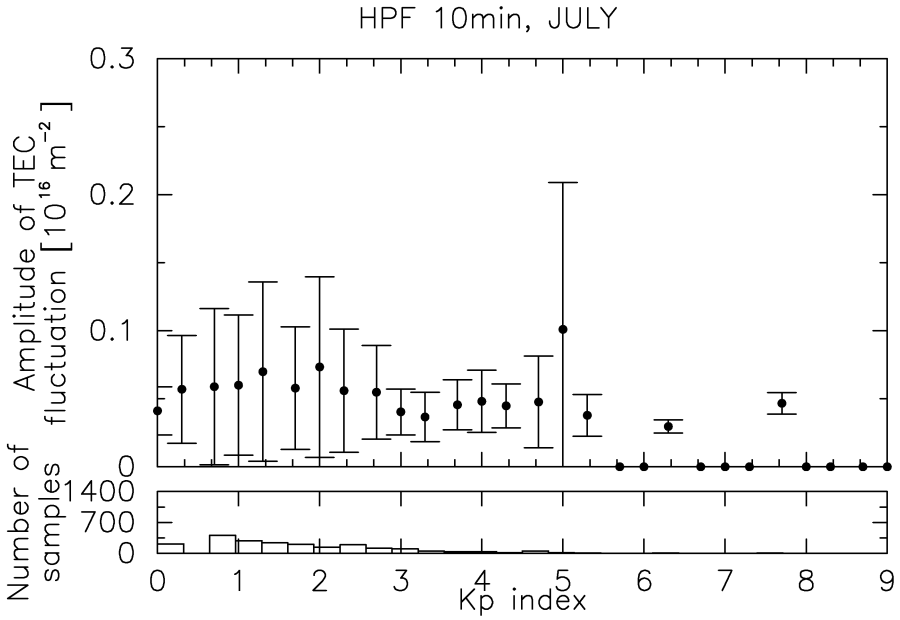

(b)

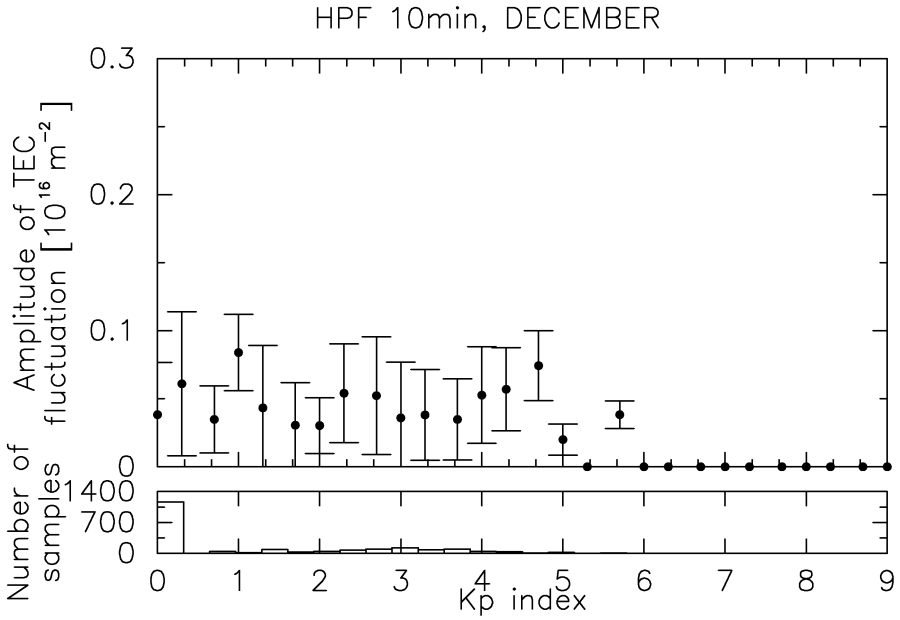

Figure 9: Dependence of the typical fluctuation amplitude of the terrestrial ionosphere on Kp index in (a) July 1999 and (b) December 1999. Standard deviation of the samples is indicated by error bars.

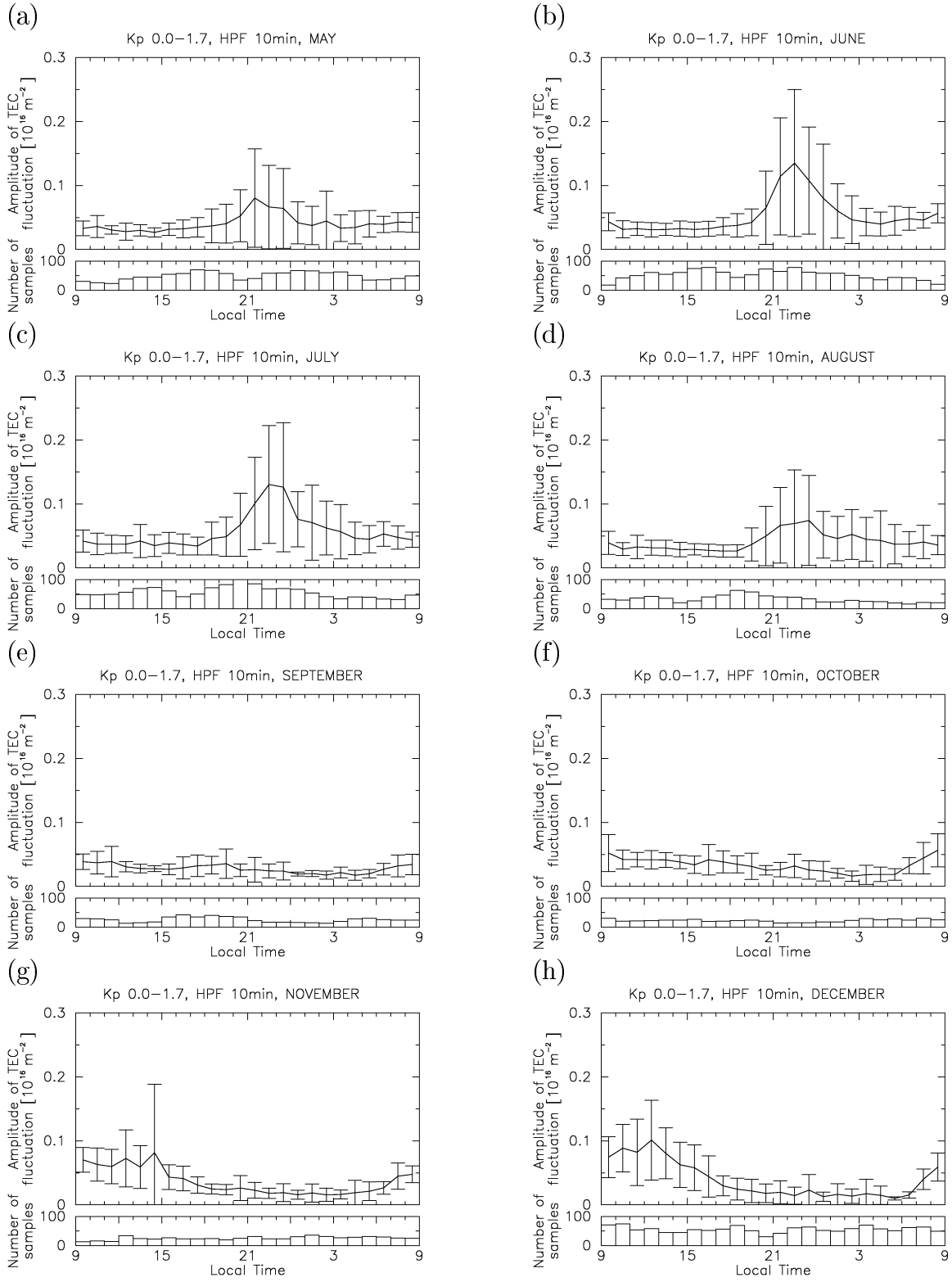

Figure 10: Dependence of the fluctuation activity of the terrestrial ionosphere on local time in (a) May 1999, (b) June 1999, (c) July 1999, (d) August 1999, (e) September 1999, (f) October 1999, (g) November 1999, and (h) December 1999. Standard deviation of the samples is indicated by error bars.

(a)

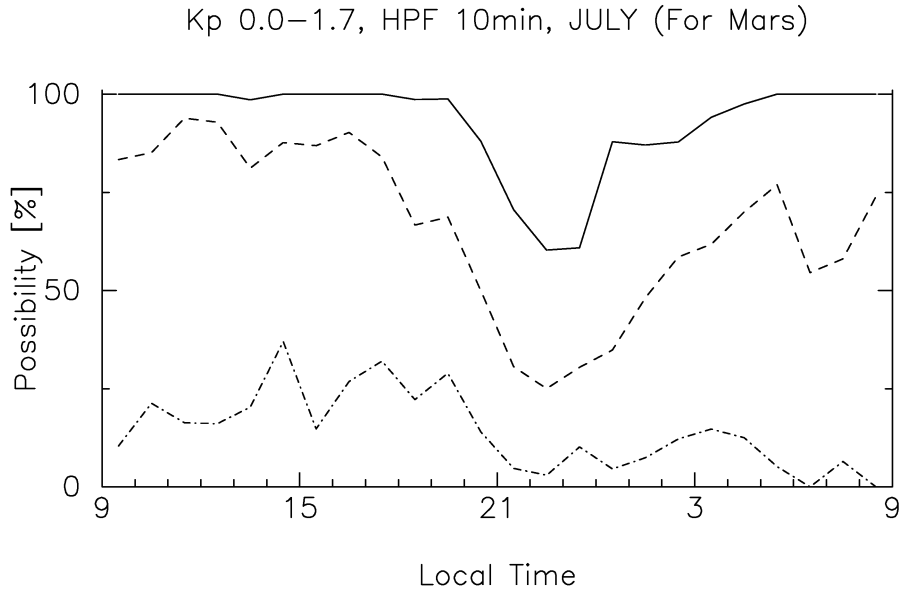

(b)

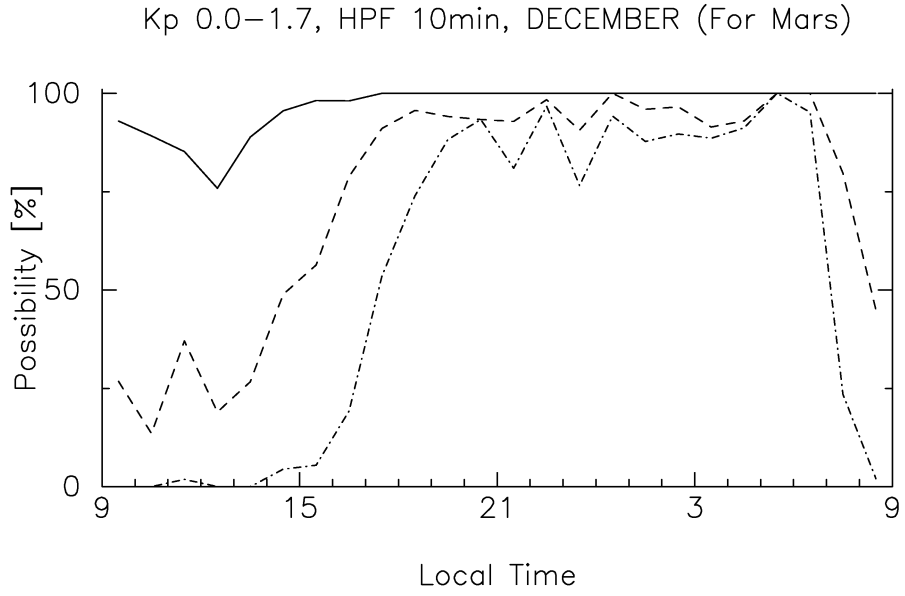

Figure 11: Possibility of the detection of the Martian nightside ionosphere in (a) July 1999 and (b) December 1999. Solid curve, dashed curve, and dot-dashed curve indicate the possibilities when the signal-to-noise ratio is required to be larger than 2, 5, and 10, respectively.

(a)

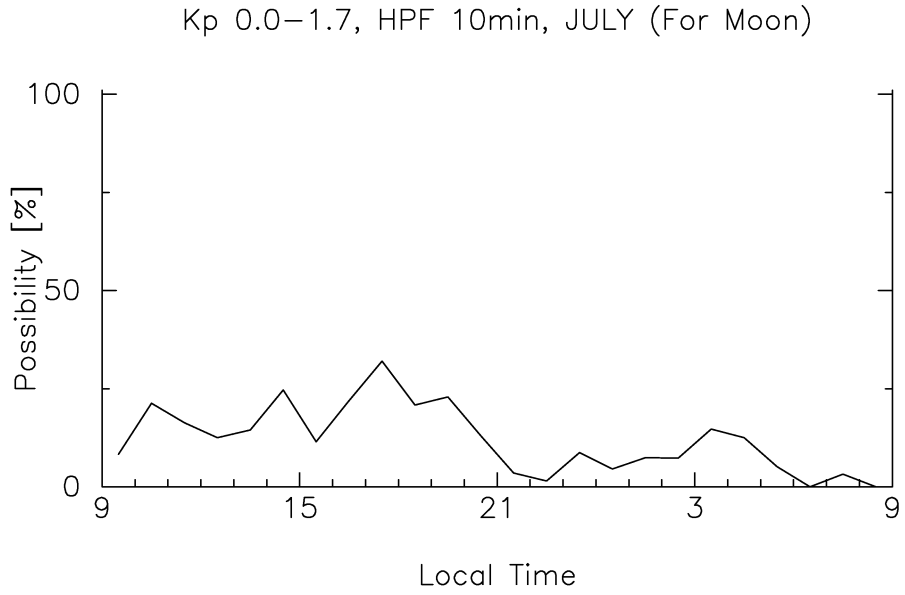

(b)

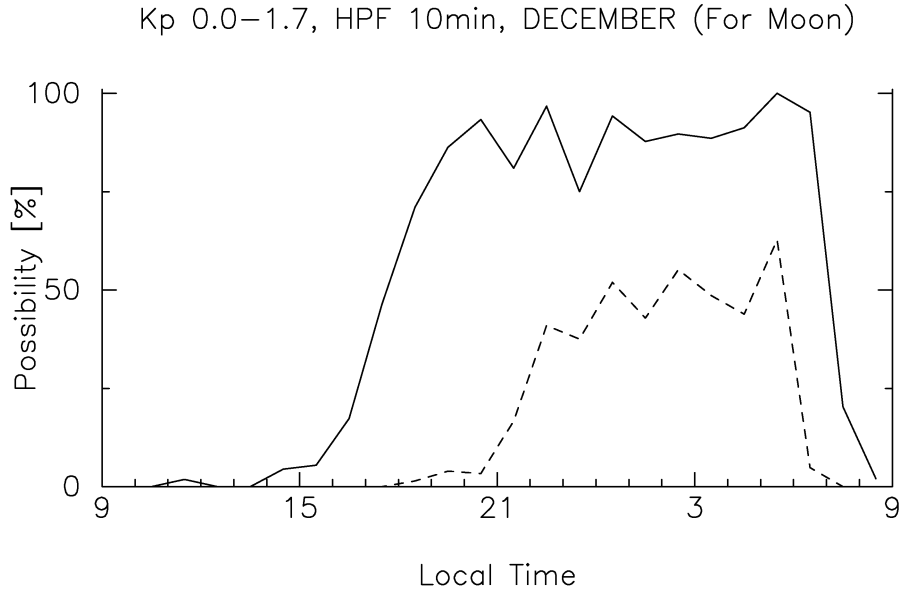

Figure 12: Possibility of the detection of the lunar ionosphere in (a) July 1999 and (b) December 1999. Solid curve and dashed curve indicate the possibilities when the signal-to-noise ratio is required to be larger than 2 and 5, respectively.

4 Estimation of the fluctuation of the terrestrial ionosphere along the ray path

In this section, a method to estimate the fluctuation of the terrestrial ionosphere along the ray path of the radio occultation is presented. For the estimation, we utilize the TEC data by the GPS network.

4.1 Method

There are several ways to estimate the fluctuation of the TEC of the terrestrial ionosphere by using the GPS network. In general, it is difficult to find a GPS satellite-ground receiver pair whose ray path is close to the ray path of the radio occultation measurement of the planetary atmosphere. Therefore, we use TEC data by many GPS satellite-ground receiver pairs to estimate the fluctuation of the terrestrial ionosphere along the ray path of the radio occultation.

We assume that the fluctuation of the terrestrial ionosphere is localized on the 300 km altitude surface, which is the altitude of the F-region peak according to the IRI90 model [*Saito et al.,* 1998]. Then, the TEC fluctuation along the ray path of each GPS satellite-receiver pair is considered to have its origin at the intersection where the ray path crosses the 300 km surface. The raw TEC data by the GPS network are the slant columns of the TEC along the ray paths from GPS satellites to ground receivers. To convert the slant column to the vertical column at the intersection, the observed TEC is multiplied by the ratio of the thickness of the ionosphere to the length of the ray path within the ionosphere, on the assumption that plasma in the ionosphere exists between 250 km and 450 km altitudes (Figure 13). The TEC value at the intersection of the ray path of the radio occultation is estimated by averaging the above TEC values inside a circle with the center at the intersection (Figure 14). The averaged value is converted to the slant TEC along the ray path of the radio occultation.

The feasibility of this method is tested by regarding one GPS satellite as the Nozomi or Selene spacecraft. The TEC data belonging to this "target GPS satellite" is not used in the above estimation procedure. The radii of the circle adopted are 20 km, 30 km, and 40 km. Since we got similar results for these radii, only the results for the 30 km radius are presented. The width of the running average to remove the trend component is 10 minutes (Section 3).

4.2 Results

An example of the feasibility test is shown in Figure 15. In this case, the satellite "No. 16" is the target satellite which gives the true TEC value, while the TEC data

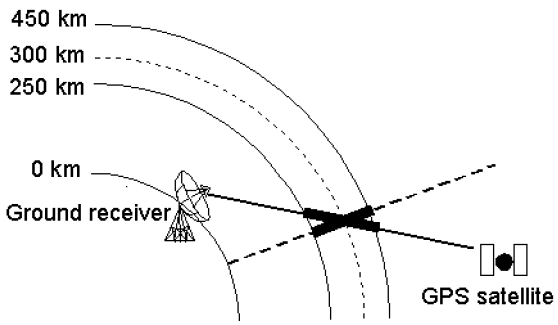

Figure 13: Conversion of the slant column to the vertical column.

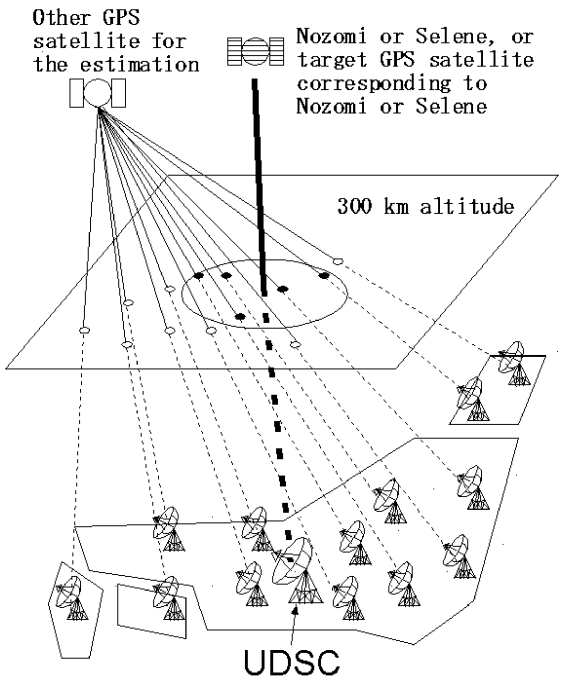

Figure 14: Method to estimate the fluctuation of the terrestrial ionosphere by using the GPS network. The TEC data inside a circle (solid symbols) are used for the estimation.

by the satellite "No. 14" is used for the estimation. The direction of the satellite No. 14 is separated from that of the satellite No. 16 by approximately 70°. Before 1600 LT, the wavelike fluctuation observed by the target satellite No. 16 is well reproduced by the estimation which uses the data obtained by the satellite No. 14. The wavelike fluctuation is caused by the movement of the ray path of the target satellite (Figure 16) across the wavelike structure of TEC (Figure 17).

After 1630 LT, the true and the estimated fluctuations are out of phase. A possible reason is that the fluctuation of the terrestrial ionosphere is no longer localized on the 300 km surface after 1630 LT. When the ray paths become longer as the satellites move to low elevations, the error caused by this assumption becomes larger. It is also possible that the altitude of the fluctuation varies spatially.

A better agreement between the true TEC and the estimated TEC is obtained as shown in Figure 18 when the altitude of the ionospheric fluctuation is assumed to be 250 km. Therefore, the most suitable surface altitude can be determined so that the difference between the TEC distributions obtained by several GPS

satellites may be minimum.

Examples of much worse results are shown in Figures 19 and 20. In the cases such that the TEC fluctuates randomly, the estimation of the TEC fluctuation along the ray path is difficult. Nevertheless, this method enables us to tell whether the radio occultation measurement is distorted by the terrestrial ionosphere or not.

If we can estimate TEC variation not only qualitatively but also quantitatively, it is possible to remove the effect of the terrestrial ionosphere from the radio occultation data. One of the bottleneck of the estimation is the sampling interval of 30 seconds. The time scale of the measurement of the Martian ionosphere and the lunar ionosphere is several minutes and several tens seconds, respectively (Section 2). Thus, much faster sampling of the terrestrial TEC is desirable.

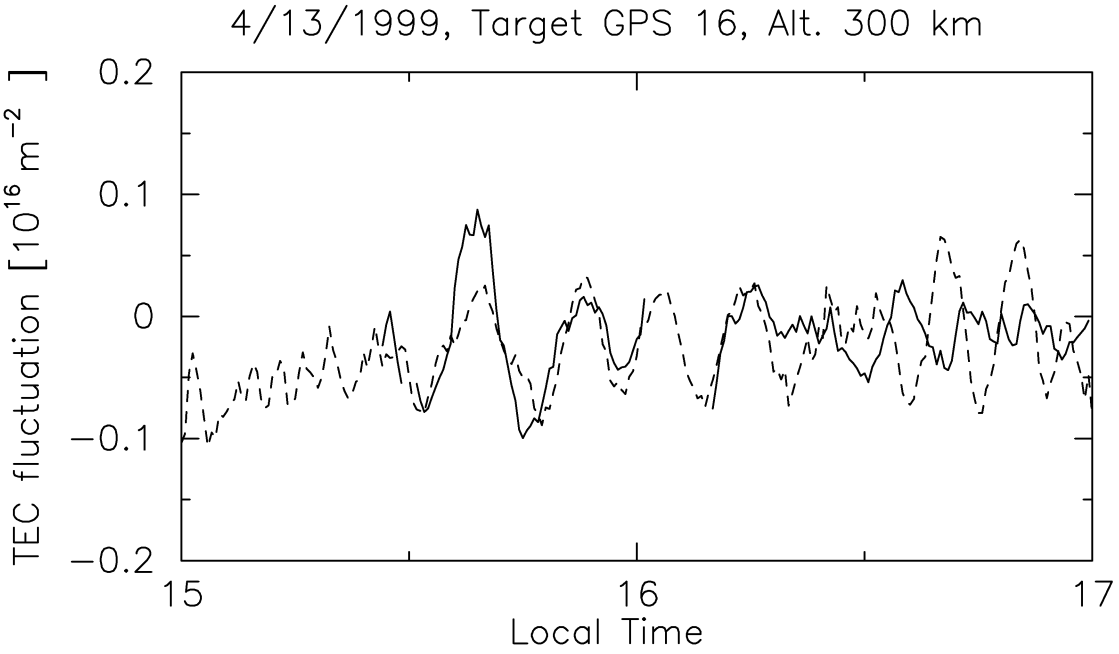

Figure 15: A feasibility test to estimate the TEC fluctuation along the ray path of a target satellite by using the TEC data observed by another GPS satellite. Dashed curve is the "true TEC" observed by the target GPS satellite No. 16, while solid curve is the "estimated TEC" which are the averages of the TEC values by the satellite No. 14 at surrounding points. The TEC fluctuation is assumed to be localized on the 300 km surface. Loss of samples near 2200 LT is due to the error of observations.

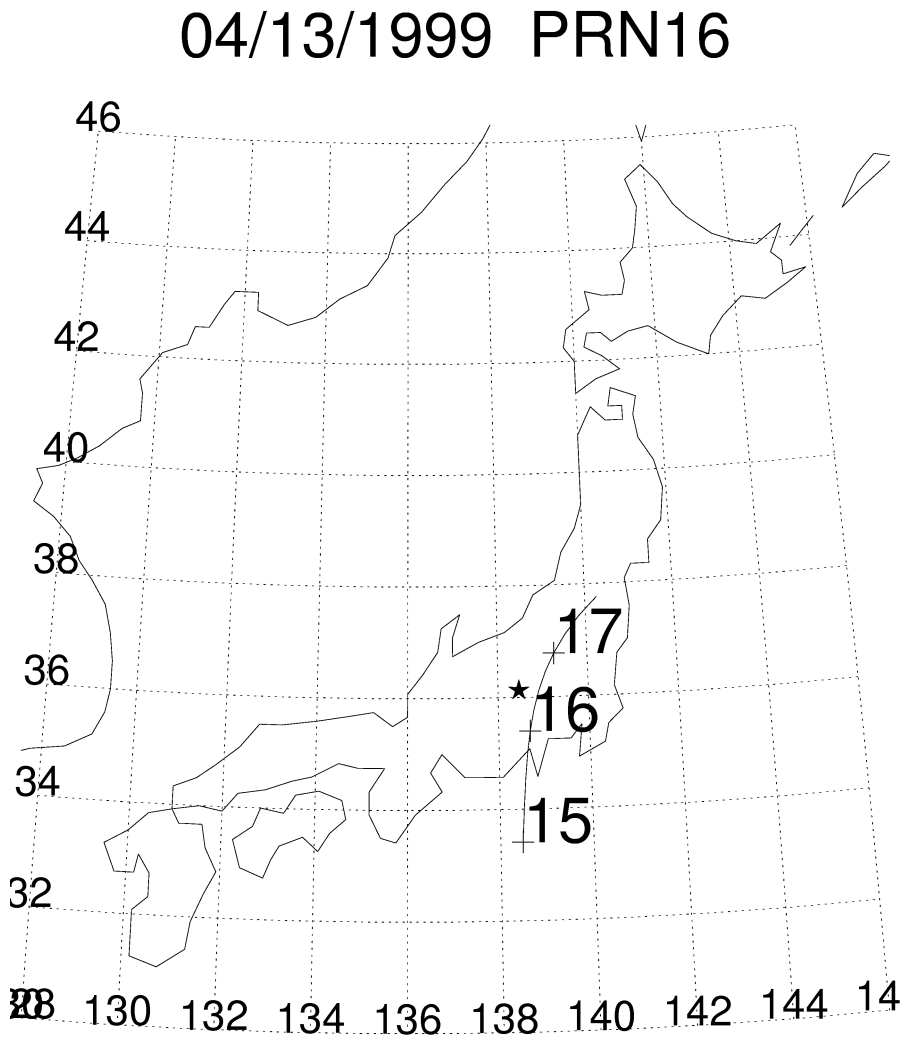

Figure 16: Trajectory of the intersection where the ray path between the GPS satellite No. 16 and UDSC crosses the 300 km altitude surface (solid curve). Star indicates the position of UDSC, and numerals on the map indicates local time, respectively.

(a)

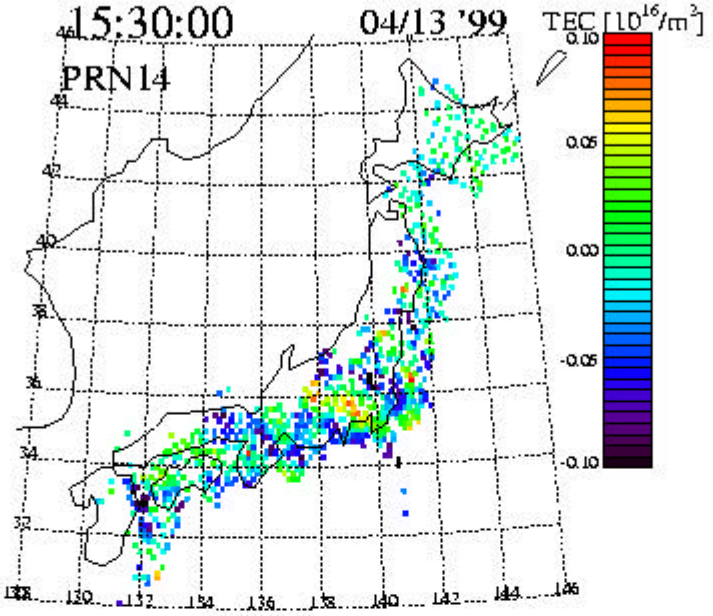

(b)

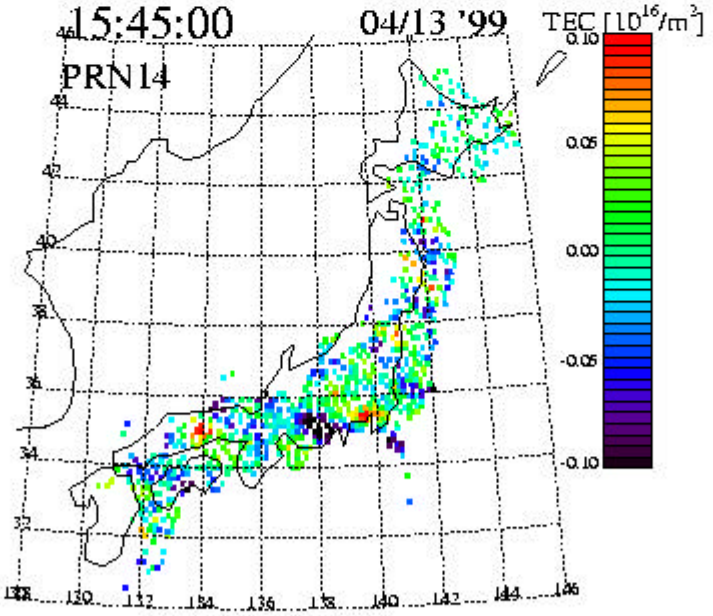

Figure 17: Two-dimensional distribution of the TEC fluctuation obtained by the GPS satellite No. 14 and 900 ground receivers at (a) 1530 LT and (b) 1545 LT. Wavelike structures is evident.

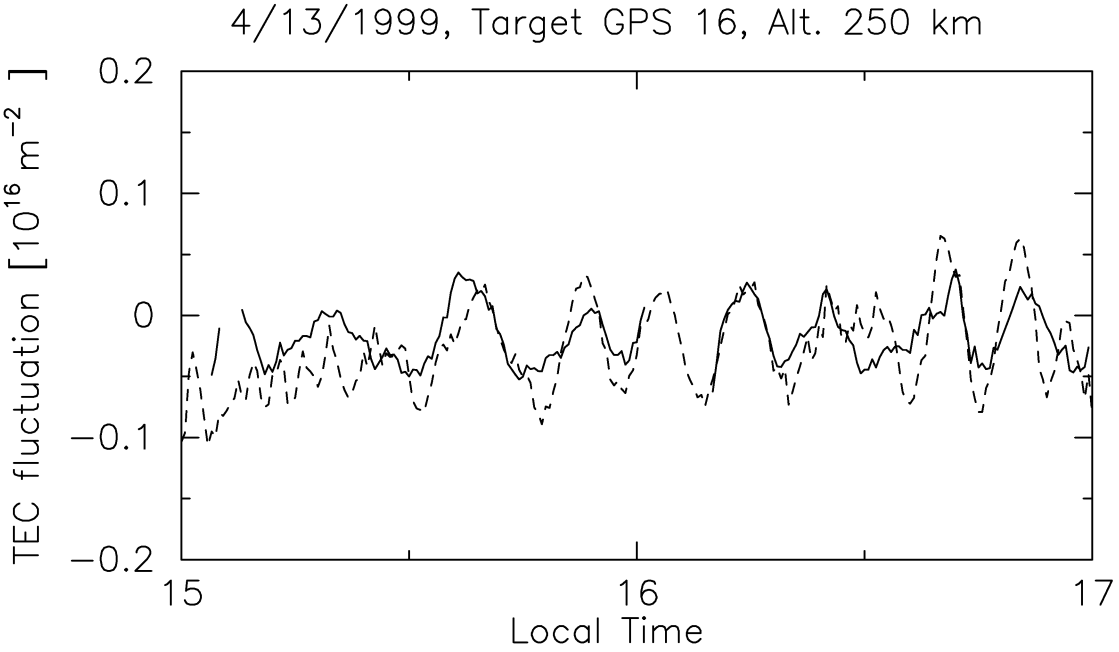

Figure 18: Same as 15, but the altitude of the ionospheric fluctuation is assumed to be 250 km.

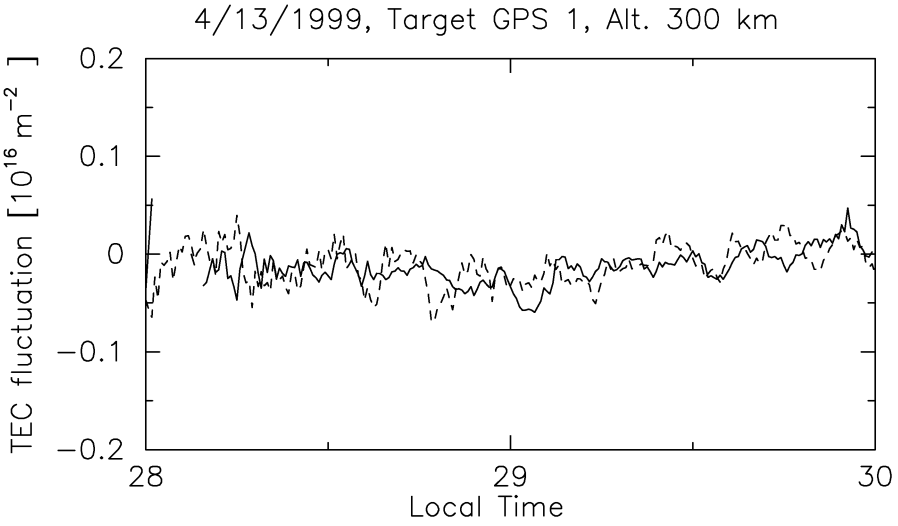

Figure 19: Same as Figure 15, but for a smaller fluctuation case.

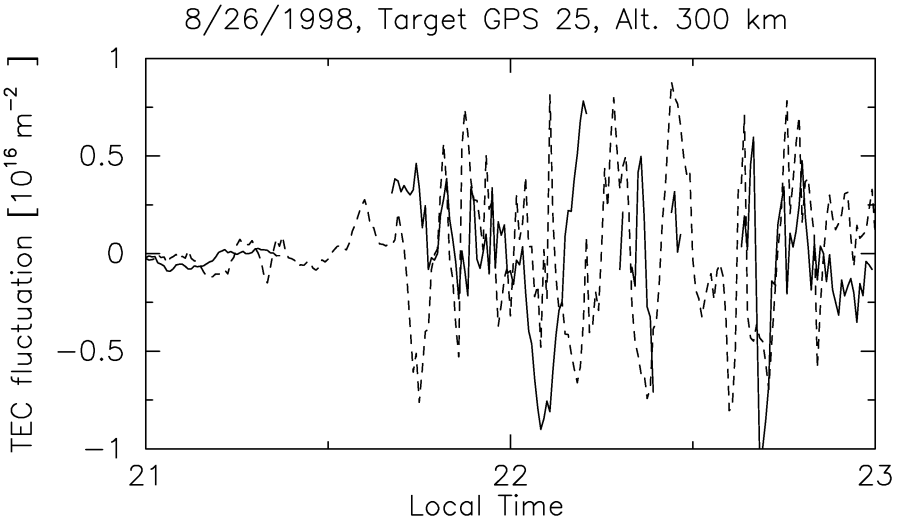

Figure 20: Same as Figure 15, but for a larger fluctuation case.

5 Summary and Conclusions

We focus on the fluctuation of the terrestrial ionosphere, which is a serious error source when we try to obtain the information on planetary ionospheres by the radio occultation measurement. In Section 2, the phase shifts caused by the radio occultations of the Martian nightside ionosphere and the lunar ionosphere are calculated. It was shown that the phase shift by the fluctuation of the terrestrial ionosphere is comparable with those by the Martian nightside ionosphere and the lunar ionosphere. In Section 3, the magnitude and the local-time dependence of the variation of the terrestrial ionosphere over the vicinity of UDSC are clarified using the TEC data obtained by the GPS network. The periods of suitable conditions for the measurement are revealed. In Section 4, the method for the estimation of the fluctuation of the terrestrial ionosphere along the ray path by using the GPS network is presented. The validity of this method is tested by regarding one GPS satellite as the Nozomi or Selene spacecrafts.

Future works to improve the lower limit of the detectability of planetary ionospheres will be:

1. To analyze the TEC data covering several years to clarify the seasonal variation of the fluctuation characteristics of the terrestrial ionosphere.

2. To increase the sampling rate of the observation of the terrestrial ionosphere by the GPS network. The fluctuations with the time scale of less than 1 minutes should be monitored if we would measure the small structures of the planetary ionosphere.

謝辞

本研究は、小山孝一郎教授の手厚い御指導のもとに完成することが出来ました。先生には、大変御多忙にも関わらず、数多くの貴重な御助言をいただき、深く感謝致します。

国土地理院の宮崎真一さん、京都大学理学部の斉藤昭則助手には、ＧＰＳによるＴＥＣデータの提供をしていただき、深く感謝致します。特に、斉藤さんには解析結果の検討について多くの御助言をいただき、ありがとうございました。

阿部琢美助教授には、惑星電離圏の研究について詳細な解説をしていただき、深く感謝致します。基本的なデータ解析手法についても御忙しい中から時間を割いて教えていただき、ありがとうございました。

今村剛助手には、本研究に留まらず、私の研究生活全般にわたって面倒を見ていただき、深く感謝致します。些細な質問にもいつも付き合っていただき、ありがとうございました。

小山研博士１年の徳山さん，吉村さん、修士２年の栗原君、山本君、修士１年の今川君、久保田君、下山君には大変御世話になりました。特に下山君には計算機のメンテナンスで色々面倒をかけました。どうもありがとう。

最後に、東北大の故若栗康宏君とは時には宇宙への夢を熱く語りながら、互いに励まし合って「のぞみ」による研究をしてきました。心から御冥福をお祈りいたします。

2000年2月

A Inverse method for radio occultation measurement

A.1 Derivation of the refractive index profile

The time series of the field intensities of S-band and X-band signals from the spacecraft is registered at the ground station. From this data the refractive index profile is obtained as follows:

1. The frequency time series is derived from the time series of the field intensity by phase unwrapping.
2. The relationship between the bending angle and the impact parameter is derived from the frequency time series.
3. The refractive index profile is derived from the relationship between the bending angle and the impact parameter.

A.1.1 Frequency time series

The time series of the field intensity $h(t)$ with the frequency f is expressed as

$$h(t) = \tilde{h} \exp[i\Phi(t)], \tag{7}$$

where $\tilde{h}$ is the real amplitude,

$$\Phi(t) = 2\pi f t + \phi_0 \tag{8}$$

is the phase at time t, and ϕ_0 is the initial phase. The Fourier transform of h at the frequency f_{FT} with the interval T centered at t is (Figure 21)

$$H(f_{FT}) = \int_{-\frac{T}{2}}^{+\frac{T}{2}} h(t+\tau) \exp[-i(2\pi f_{FT}\tau)] d\tau$$

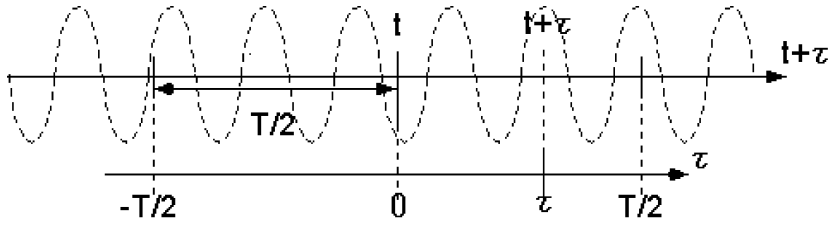

Figure 21: Concept of Fourier transform with a finite interval.

$$
\begin{aligned}
&= \tilde{h}\exp[i(2\pi ft+\phi_0)]\int_{-\frac{T}{2}}^{+\frac{T}{2}}\exp[i2\pi(f-f_{FT})\tau]d\tau \\
&= \tilde{h}\exp[i(2\pi ft+\phi_0)]\frac{\sin(\pi(f-f_{FT})T)}{\pi(f-f_{FT})} \\
&= A\exp[i\Phi(t)], \qquad (9)
\end{aligned}
$$

where

$$A = \tilde{h}\frac{\sin(\pi(f-f_{FT})T)}{\pi(f-f_{FT})}. \qquad (10)$$

Since A is real, the signal phase at time t is obtained as

$$\Phi(t) = \tan^{-1}\frac{\mathrm{Im}[H(f_{FT})]}{\mathrm{Re}[H(f_{FT})]}. \qquad (11)$$

Note that the result does not depend on the choice of f_{FT}. In the actual data processing where discrete Fourier transform is used, f_{FT} is set at the frequency bin which gives the maximum power in the discrete spectrum. The frequency of the signal can be obtained from the finite difference of the phase in short time interval Δt,

$$f = \frac{\Phi(t+\Delta t)-\Phi(t)}{\Delta t}. \qquad (12)$$

Since the received signal has been down-converted during data sampling by mixing the synthesizer signal, the frequency of the received signal f_{obs} is obtained as

$$f_{obs} = f + f_{synth}, \qquad (13)$$

where f_{synth} is the synthesizer frequency. The phase unwrapping method described above is applied after lowering the noise level by a narrow band-pass filter.

A.1.2 Relationship between the bending angle and the impact parameter

The radio wave emitted from the spacecraft is received by the earth-based antenna after the refraction in the planetary atmosphere (Figure 22). The angle θ between the ray path of the radio wave emitted from the spacecraft and the velocity vector of the spacecraft depends on the bending angle α. Thus, the Doppler shift $\delta f_{s/c}$ due to the motion of the spacecraft depends on α. If $\delta f_{s/c}$ is measured, α can be obtained.

The Doppler shift $\delta f_{s/c}$ is related to f_{obs} as

$$f_{obs} = f_{USO} + \delta f_{s/c} + \delta f_{rel} + \delta f_{ant}, \qquad (14)$$

where f_{USO} is the frequency of the radio wave emitted from the spacecraft (the nominal frequency), δf_{rel} is the frequency shift due to the gravity field of the Sun and planets, and δf_{ant} is the Doppler shift due to the motion of the earth-based receiver. Thus, $\delta f_{s/c}$ can be obtained if f_{USO}, δf_{rel}, and δf_{ant} are known and f_{obs} is measured as described in the previous section[2]. The dependence of $\delta f_{s/c}$ on θ is expressed as

$$\delta f_{s/c} = f_{USO} \frac{v_s \cos\theta}{c}, \tag{15}$$

where v_s is the spacecraft velocity and c is the light velocity in vacuum. By using (15) the angle θ is obtained from $\delta f_{s/c}$. When the angle θ and the coordinates of the planet, the spacecraft and the earth-based receiver are known, the impact parameter a and the bending angle α can be obtained geometrically.

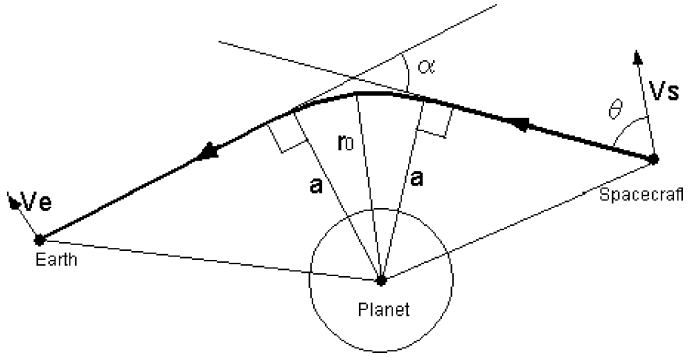

Figure 22: Geometry of the radio occultation measurement

A.1.3 Refractive index profile

We can obtain the refractive index profile from the relationship between the bending angle α and the impact parameter a by solving the inverse problem [*Fjeldbo et al.,* 1971]. The refractive index profile is obtained as

$$\mu(r_{01}) = \exp\left[-\frac{1}{\pi}\int_{\alpha=\alpha(a_1)}^{\alpha=0} ln\left[\frac{a(\alpha)}{a_1} + \left\{\left(\frac{a(\alpha)}{a_1}\right)^2 - 1\right\}^{\frac{1}{2}}\right] d\alpha\right], \tag{16}$$

where a_1 is the impact parameter of the ray path whose closest distance is r_{01}. (16) is expressed also as

$$\mu(r_{01}) = \exp\left[-\frac{1}{\pi}\int_{a=a_1}^{a=\infty} ln\left[\frac{a}{a_1} + \left\{\left(\frac{a}{a_1}\right)^2 - 1\right\}^{\frac{1}{2}}\right] \frac{d\alpha}{da} da\right]. \tag{17}$$

[2] δf_{ant} depends on α in a manner similar to $\delta f_{s/c}$. However, since the distance between the earth-based receiver and the planet is much longer than that between the spacecraft and the planet, the dependence of δf_{ant} on α is negligible.

In general, a is multivalued function of α. Therefore the formulation (17) is preferred rather than (16).

A.2 Derivation of profiles of the electron density and the neutral atmosphere

In this section we obtain the density profiles of the neutral atmosphere and the electron in the ionosphere from the refractive index profile. Both of the neutral atmosphere and the ionosphere contribute to the refractive index. They can be separated when two frequency channels are available by utilizing the difference of the frequency dependence of the refractive index between plasma and neutral gases.

The refractive index μ is expressed as

$$\mu = \frac{c}{v_\phi}, \tag{18}$$

where v_ϕ is the phase velocity of the radio wave. The dispersion relation of the electromagnetic waves in an unmagnetized plasma is expressed as [*Kivelson et al.*, 1995]

$$\omega^2 = c^2k^2 + {\omega_p}^2, \tag{19}$$

where ω is the angular frequency of the radio wave and k is the wave number, and ω_p is the plasma frequency. ω_p is defined as

$${\omega_p}^2 = \frac{N_e e^2}{m_e \varepsilon_0}, \tag{20}$$

where N_e is the electron density, e is the elementary charge, m_e is the mass of electron, and ε_0 is the permittivity of vacuum. Using (18), (19), (20), and the relationship $v_\phi = w/k$, we obtain the refractive index of plasma as

$$\mu \simeq 1 - \frac{e^2}{8\pi^2 m_e \varepsilon_0}\frac{N_e}{f^2} \tag{21}$$

$$\simeq 1 - 40.3\frac{N_e}{f^2}, \tag{22}$$

where Ne is in m^{-3} and f is the frequency of the radio wave in Hz. On the other hand, the refractive index of the neutral gas does not depend on the frequency:

$$\mu = 1 + N_m, \tag{23}$$

where v is proportionality constant known as *refractive volume* and N_m is the molecular number density.

The refractive index profiles are assumed to be obtained both for S-band and X-band. From (22) and (23), the refractive indexes in S-band and X-band are expressed as

$$\mu_S = 1 + vN_m - \frac{e^2}{8\pi^2 m_e \varepsilon_0}\frac{N_e}{f_S^2}, \tag{24}$$

$$\mu_X = 1 + vN_m - \frac{e^2}{8\pi^2 m_e \varepsilon_0}\frac{N_e}{f_X^2}, \tag{25}$$

where the subscripts S and X denote S-band and X-band, respectively. Using (24) and (25), we can obtain the electron density and the molecular number density from the refractive indexes as

$$N_e = \frac{8\pi^2 m_e \varepsilon_0}{e^2}\frac{f_S^2 f_X^2}{f_S^2 - f_X^2}(\mu_S - \mu_X), \tag{26}$$

$$N_m = \frac{f_S^2(\mu_S - 1) - f_X^2(\mu_X - 1)}{v(f_S^2 - f_X^2)}. \tag{27}$$

In the Nozomi mission, we can not use the S-band downlink due to the trouble of power supply (Section 1). However, the contributions of the ionosphere and the neutral atmosphere of Mars in the data are expected to be separated easily since they are separated in altitude.

References

Aarons, J.,M. Mendillo, R. Yantosca, and E. Kuaeki, GPS phase fluctuations in the equatorial region during the MISETA 1994 campaign, *J. Geophys. Res.,101*, 26851-26862, 1996.

Aarons, J., Global positioning system phase fluctuations at auroral latitudes, *J. Geophys. Res., 102*, 17219-17231, 1997.

Bauer, S. J., Limits to a Lunar Ionosphere, *Anzeiger Abt, II, 133*, 17-21, 1996.

Doherty, P. H., E. Raffi, J. A. Klobuchar, and M. B. El-Arini, Statistics of time rate of change of ionospheric range delay, *Proc. Iono. Global Positioning System Inst. of Navig.*, 1589-1598, 1994.

Fjeldbo, G., and V. R. Eshleman, The bistatic radar-occultation method for the study of planetary atmospheres, *J. Geophys. Res., 70*, 3217-3225, 1965.

Fjeldbo, G., and V. R. Eshleman, The atmosphere of Mars analyzed by integral inversion of the Mariner IV occultation data, *Planet Space Sci., 16*, 1035-1059, 1968.

Fjeldbo, G., A. J. Kliore, and V. R. Eshleman, The neutral atmosphere of the Venus as studied with the Mariner V radio occultation experiments, *The Astronomical J., 76*, 123-140, 1971.

Fox, J. L., and J. F. Brannon, Upper limits to the nightside ionosphere of Mars, *Geophys. Res. Let., 20, 13*, 1391-1394, 1993.

Haider, S. A., J. Kim, A. F. Nagy, C. N. Keller, M. I. Verigin, K. I. Gringauz, N. M. Shutte, K. Szengo, and P. Kiraly, Calculated ionization rates, ion densities, and airglow emission rates due to precipitating electrons in the nightside ionosphere of Mars, *J. Geophys. Res., 97*, 10637-10641, 1992.

Hernandez-Pajares M., J. M. Juan, J. Sanz, and J. G. Sole, Global observation of the ionospheric electronic response to solar events using ground and LEO GPS data, *J. Geophys. Res., 103*, 20789-20796, 1998.

Hinson, D. P., R. A. Simpson, J. D. Twicken, G. L. Tyler, and F. M. Flasar, Initial results from radio occultation measurements with Mars Global Surveyor, *J. Geophys. Res., 104*, 26997-27012, 1999.

Hogan, J. S., R. W. Stewart, and S. I. Rasool, Radio occultation measurements of the Mars atmosphere with Mariners 6 and 7, *Radio Sci., 7*, 525-537, 1972.

Kivelson, M. G. and C. T. Russell, *Introduction to space physics*, Cambridge university press, 1995.

Kliore, A. J., G. Fjeldbo, B. L. Seidel, M. J. Sykes, and P. M. Woiceshyn, S band radio occultation measurements of the atmosphere and topography of

Mars with Mariner 9: Extended mission coverage of polar and intermediate latitudes, *J. Geophys. Res., 78*, 4331-4351, 1973.

Knudsen, W. C., K. Spenner, K. L. Miller, and V. Novak, Transport of ionospheric O^+ ions across the Venus terminator and implications, *J. Geophys. Res., 85*, 7803-7810, 1980.

Knudsen, W. C., and K. L. Miller, Pioneer Venus suprathermal electron flux measurements in the Venus umbra, *J. Geophys. Res., 90*, 2695-2702, 1985.

Knudsen, W. C., The Venus ionosphere from in situ measurements, *Venus and Mars: Atmosphere, Ionosphere, and Solar Wind Interactions, Geophysical Monograph 66*, AGU, 237-263, 1992.

Lindal, G. F., H. B. Hotz, D. N. Sweetnam, Z. Shippony, P. Brenkle, G. V. Hartsell, R. T. Spear, and W. H. Michael, Jr., Viking radio occultation measurements of the atmosphere and topography of Mars: Data acquired during 1 Martian year of tracking, *J. Geophys. Res., 84*, 8443-8456, 1979.

Mizuno, E., Coherent signal arraying of Voyager-Neptune radio occultation data: Data analysis and improvement of physical measurements, *Doctoral dissertation*, University of Tokyo, 1991.

Phinney, R. A., and D. L. Anderson, On the radio occultation method for studying planetary at atmospheres, *J. Geophys. Res., 73*, 1819-1827, 1968.

Reasoner, D. L., and W. J. Burke, Direct observation of the lunar photoelectron layer, *Proceeding of the Third Science Conference, 3*, 2639-2654, 1972.

Saito, A., S. Fukao, and S. Miyazaki, High resolution mapping of The perturbations with the GSI GPS network over Japan, *Geophys. Res. Let., 25, 16*, 3079-3082, 1998.

Savich, N. A., V. A. Samovol, M. B. Vasilyev, A. S. Vyshlov, L. N. Samoznaev, A. I. Sidorenko, and D. Ya. Shtern, The nightside ionosphere of Mars from Mars-4 and Mars-5 radio occultation dual-frequency measurements, *NASA-SP, 397*, 41-46, 1976.

Sutte, N., K. Gringauz, P. Kiraly, G. Kotova, A. F. Nagy, H. Rosenbauer, K. Szego, and M. Verigin, Nightside electron flux measurements at Mars by Phobos-2 HARP instrument, *Geophys. Res. Let., 22, 7*, 863-866, 1995.

Stern, S. A., The lunar atmosphere: History, status, current problems, and context, *Rev. of Geophys., 37*, 453-491, 1999.

Verigin, M. I., K. I. Gringauz, N. M. Shutte, S. A. Haider, K. Szego, P. Kiraly, A. F. Nagy, and T. I. Gombosi, On the possible source of the ionization in the nighttime Martian ionosphere 1. Phobos 2 HARP electron spectrometer measurements, *J. Geophys. Res., 96*, 19307-19313, 1991.

Vyshlov, A. S., Preliminary results of circumlunar plasma research by Luna22 spacecraft, *Space Res., XVI*, 945-949, 1976.

Woo, R. and J. W. Armstrong, Spacecraft radio scattering observations of the power spectrum of electron density fluctuations in the solar wind, *J. Geophys. Res., 84*, 7288-7296, 1979.

Zhang, M. H. G., J. G. Luhmann, and A. J. Kliore, An observational study of the nightside ionosphere of Mars and Venus with radio occultation methods, *J. Geophys. Res., 95*, 17095-17102, 1990.